J. Min. Metall. Sect. B-Metall. 58 (2) (2022) 321 - 333

Journal of Mining and Metallurgy, Section B: Metallurgy

HOT DEFORMATION BEHAVIOR OF MICRO-ALLOYED STEEL USING PROCESSING MAPS DEVELOPED WITH DIFFERENT CONSTITUTIVE EQUATIONS

S. K. Thakur [a,b,*], A. K. Das [b], B. K. Jha [c]

[a] Steel Authority of India Ltd., R&D Centre for Iron & Steel, Ranchi, India
[b] IIT(ISM), Mechanical Engineering, Dhanbad, India
[c] National Institute of Foundry & Forge Technology (NIFFT), Department of Materials & Metallurgy, Ranchi, India

(Received 14 January 2022; Accepted 07 July 2022)

Abstract

The hot workability of microalloyed steel was studied in the deformation temperature range of 850 – 1200°C and strain rate of 0.001-100s^{-1}. The constitutive relation of flow stress with temperature, strain rate and strain was established to construct processing maps of the microalloyed steel. The processing maps were constructed using conventional power law, integral method, and Arrhenius equations. The developed processing maps were used to predict the optimal hot deformation conditions and were validated with metallurgical examinations. The safe regime for hot working of the experimental steel was found to be in the intermediate temperature-strain rate range (1000-1150°C;0.001-10 s^{-1}), where the deformation process was dominated by dynamic recrystallization and dynamic recovery of the austenitic phase. The processing map constructed using Arrhenius equations increased continuously with an increase in deformation temperature and decrease in strain rate and it did not reveal relevant information of hot workability with respect to deformation temperature and strain rate. The dynamic recrystallization behavior of experimental steel was affected by both deformation temperature and strain rate which was explained in detail through microstructural examination.

Keywords: *Deformation; Processing map; Microalloyed; Arrhenius equation*

1. Introduction

Workability of the material prescribes the limit on the amount of deformation a workpiece can withstand at a given strain rate and temperature. The selection of improper processing parameters may generate defects in the form of macroscopic cracks and other instabilities during hot working. Hot workability depends on a material parameter such as chemical composition, microstructure, thermo-mechanical history, and external processing parameters [1]. Hot rolling of the steel is carried out in the temperature range of 800-1200°C and it involves deformation at high strain rates. Deformation of steel at such high temperatures and strain rates are associated with microstructural evolution during processing. Thus, understanding the steel behavior during hot deformation is essential in controlling the microstructure and optimizing the hot deformation process.

Processing maps are extensively used to optimize the hot deformation process and achieve the desired microstructure for safe working and the desired mechanical properties without trial and error, as well as determining process limitations in the manufacturing process [2-4]. Prasad etal. developed the processing map based on the theory of the Dynamic Material Model (DMM) [5-6]. The methodology describes the dynamic path that a material element follows with respect to changes in effective strain rate at a given temperature and effective strain. In DMM, the workpiece is assumed to dissipate power during hot deformation. It also assumes a visco-plastic material and its constitutive response during hot deformation is mainly strain rate dependent. The flow stress during hot deformation is represented by the power-law constitutive equation as given in equation (1):

$$\sigma = K \dot{\varepsilon}^{m} \tag{1}$$

where, K is material constant, m is strain rate sensitivity, σ is flow stress of the material, and $\dot{\varepsilon}$ represents the strain rate. The power-law constitutive equation is not valid for higher strain rates and

Corresponding author: skthakur@sail.in

https://doi.org/10.2298/JMMB220114014T

complex alloy design. Murty [7] proposed an integral method for constructing processing map that is suitable for any metals and alloys, as it describes constitutive relationships between σ, ε, and $\dot{\varepsilon}$. Based on the advantages of this method, it was also used to develop processing maps in this work. The hyperbolic sine Arrhenius type constitutive equations are also well accepted to describe the relationship between the σ, $\dot{\varepsilon}$, and temperature [8]. Recently, hyperbolic sine Arrhenius type constitutive equation has been proposed as a novel computing method for processing map for Titanium alloys [9]. This method has not yet been explored for micro-alloyed steel. Zhao etal. compared power dissipation maps constructed by a various method including Arrhenius equations for 40CrNi steel and concluded that power dissipation efficiency mainly depends on the σ-$\dot{\varepsilon}$ relationship [10]. According to Zhao etal., the power dissipation map based on power-law reflected more meaningful information, whereas Arrhenius constitutive equations resulted in a monotonic efficiency pattern.

In the present work, the hot workability of microalloyed steel of 0.08C-1.2Mn-0.1Si chemistry was evaluated by developing processing maps based on the traditional power law developed by Prasad etal., the integral method developed by Murthy etal., and hyperbolic sine Arrhenius type constitutive equation. A comparative study of all three methods was done and the best method was adopted to determine the optimum hot deformation parameters.

This experimental steel belongs to the class of micro-alloyed steel which is used extensively in structural, shipbuilding, and penstock. It has unique properties of higher yield strength with good toughness. Niobium, Vanadium, and Titanium are added as micro-alloyed elements to increase the strength of these steel through grain refinement and precipitation strengthening [11-12]. These steels are rolled using Thermo-Mechanical Control Processing (TMCP) technique to improve the overall mechanical properties by controlling the hot-deformation processes. Thus, it is important to determine reasonable optimum hot deformation parameters to produce defect-free steel.

2. Experimental

The microalloyed steel sample for experimentation was collected from Plate Mill, Rourkela Steel Plant. The chemical composition of the steel is mentioned in Table 1. The microstructure of the as-received sample is shown in Fig.1 and the average ferrite grain size was around 12µm. It consisted of a typical ferrite pearlite phase. The cylindrical samples f10mmx15mm in size were fabricated for conducting hot compression tests in Gleeble-3500. The detail of the experiment is depicted in Fig.2. The strain rates varied from 10^{-3} to $10^{2}s^{-1}$ and deformation temperature was kept in the range of 850-1200°C. All tests were continued to a strain of 0.5 as most of the plate rolling of microalloyed steel was done in the strain range of 0.3-0.5. Temperature rise during deformation was taken into account and necessary corrections were incorporated while plotting true stress vs. true strain curves based on the procedure described by Goetz et.al [13]. The obtained flow curves at different strain rates and temperatures served as the basis for evaluating the efficiency of

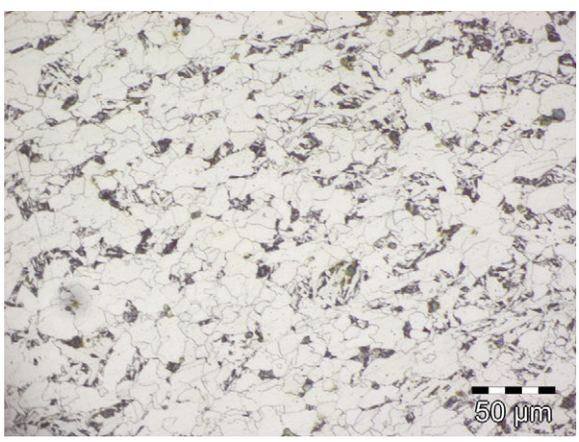

Figure 1. *Microstructure of as-rolled sample*

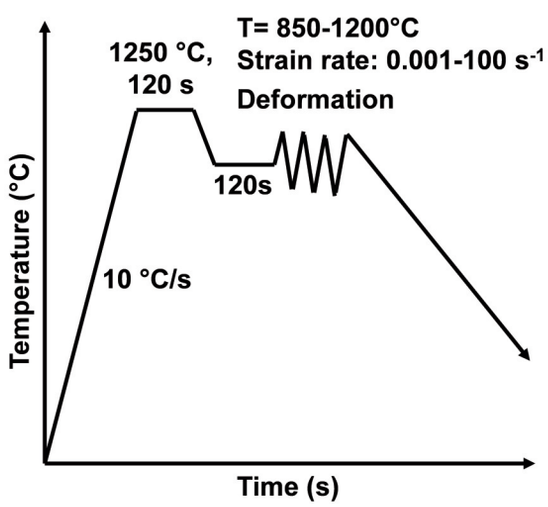

Figure 2. *Deformation process during hot compression test*

Table 1. *Chemical composition of experimental steel in weight percentage*

C	Mn	S	P	Si	Nb	V	Ti	Fe
0.08	1.2	0.01	0.015	0.1	0.05	0.07	0.02	Balance

power dissipation. The samples were split longitudinally and viewed in the optical microscope to observe structural changes that took place during the deformation. The performed microstructural analysis was carried out using DM600 M Leica Optical Microscope. The Scanning Electron Microscopy (SEM) was done using a field emission scanning electron microscope (FE-SEM, ZEISS ULTRA 55), operated at 15 kV. The deformed samples, after polishing by colloidal Silica suspension, were investigated through the use of Electron Back-Scattered Diffraction (EBSD) operated at an acceleration voltage of 20 Kev. Transmission Electron Microscopy (TEM) characterizations were performed with a Philips CM 200 FEG electron microscope using an accelerating voltage of 200 KV.

3. Results & Discussions

3.1. Flow Stress Curves

Fig. 3(a)- 3(b) depict the true stress–true strain curves of the experimental steel at different strain rates. The curves showed typical characteristics, i.e. the flow stress increased with increasing strain rate and decreased with increasing temperature. At a given strain rate and deformation temperature, the flow stress increased rapidly with an increase in strain due to increased work hardening. Dynamic softening due to dynamic recovery and dynamic recrystallization occurred after critical strain rate and countered the strain hardening effect to result in steady flow stress. It was observed that dynamic softening was sluggish at a low deformation temperature and a high strain rate due to restricted grain boundary mobility at a lower temperature, and limited time for the nucleation and growth of dynamically recrystallized grains at a higher strain rate.

3.2. Processing Map

The total power (P) during hot working was divided into two complementary parts: G and J. The power dissipation due to plastic deformation was known as G content and was represented in equation (2). The power dissipated through the microstructure change was known as J co-content and was shown in equation (3). When the work-piece worked as an ideal linear dissipater, the J reached its maximum value (J = Jmax = sé/2).

$$G = \oint_0^{\varepsilon'} \sigma d\varepsilon' \tag{2}$$

$$J = \oint_0^{\sigma} \varepsilon' d\sigma \tag{3}$$

3.3. Power Law

Prasad et al. [6] assumed that the relationship between flow stress σ and strain rate ε˙ obeyed the power law equation and the strain rate sensitivity (m) determined the amount of power dissipated through deformation and microstructure changes. The m was expressed as given in equation (4):

$$\mathrm{m} = \left[\frac{\partial \mathrm{J}}{\partial \mathrm{G}}\right]_{\varepsilon,\mathrm{T}} = \left|\frac{\partial \ln \sigma}{\partial \ln \dot{\varepsilon}}\right|_{\varepsilon,T} \tag{4}$$

The power dissipation characteristics by microstructural changes under different temperature and strain rate were represented in terms of efficiency (h) and were defined as equation (5):

$$\eta = J / Jmax = 2m/(m+1) \tag{5}$$

The plot of η with respect to temperature and strain rate was known as the power dissipation map. The η contours in the power dissipation map represented the power dissipated due to microstructural changes during hot deformation. Further, the flow instability parameter (ξ) representing metallurgical instability was determined and superimposed with the power dissipation map to

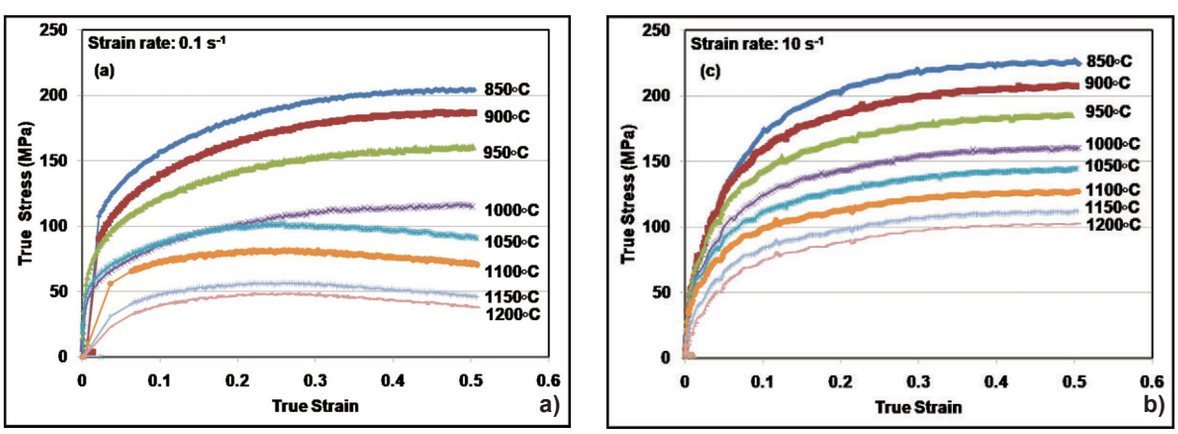

Figure 3. *True stress- true strain curves of experimental steel at strain rates (a) 0.1 s^{-1}, (b) 10 s^{-1}*

constitute the processing map along with the power dissipation map. ξ was determined using equation (6).:

$$\xi\left(\dot{\varepsilon}\right)=\frac{\partial \ln\left(\frac{m}{m+1}\right)}{\partial \ln \dot{\varepsilon}}+m<0 \quad (6)$$

Thus, the variation of ξ with temperature and strain rate constituted the instability map and flow instability was represented by an area with negativex. Based on the computation of strain rate sensitivity (m) and efficiency (η) of power dissipation during deformation, complete processing maps for microalloyed steel was constructed for strains ranging from 0.3 to 0.5 and shown in Fig.4(a)-4(c). The iso-efficiency contour in the power dissipation map represented a dynamic metallurgical condition of the material and the shaded area depicted the instability zone. The domain-B was shown in the deformation map as the highest efficiency of 50% and it occurred in the temperature range 1150-1200°C and strain rate range 0.001-0.02. The highest efficiency region not necessarily represented the safe microstructural state during hot deformation. It may be associated with internal defects such as wedge cracking and the generation of new surfaces and this can be validated with microstructure studies.

The domains with medium efficiency are normally associated with dynamic recrystallization and dynamic recovery and they represent the safe region for hot deformation. The domain-A shown in deformation maps (Fig.4) represents the iso-efficiency curves where η varied in the range of 26-33%. The temperature and strain rate range of domain-A were1000-1150°C and 0.001-100 s^{-1}respectively. Domain-A represented the safe region with the dominance of dynamic recovery and recrystallization during hot deformation. The material exhibited flow instability (Domain-C) in the temperature range 850-1150°C when the strain rate was> 1 s^{-1}. The η curve in this zone was normally less and varied in the range of 2-20%. This region depicted the unsafe condition during hot deformation.

3.4. *Arrhenius Equation*

The following constitutive Arrhenius equations (7-9) represent the relationship among flow stress, temperature, and strain rate [14, 15].

$$\dot{\varepsilon}=A1\sigma^{n1}\exp\left(\frac{-Q_{def}}{RT}\right),\alpha\sigma\le 0.8 \quad (7)$$

$$\dot{\varepsilon}=A2\exp(\beta\sigma)\cdot\exp\left(\frac{-Q_{def}}{RT}\right),\alpha\sigma\ge 1.2 \quad (8)$$

$$\dot{\varepsilon}=A[\sinh(\alpha\sigma_p)]^n\cdot\exp\left(\frac{-Q_{def}}{RT}\right) \quad (9)$$

where: *A, A1, A2, β, n1, α (*β/n1), and *n* are

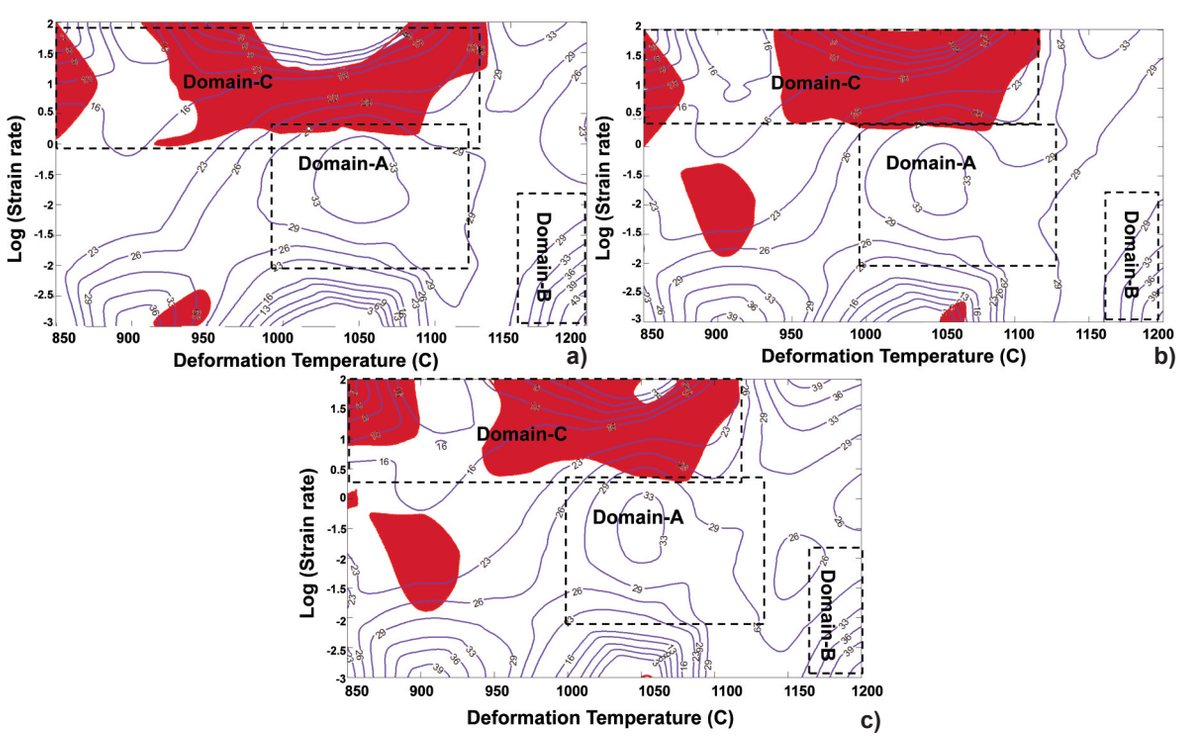

Figure 4. *Processing map using power law at 0.3 strain (a), at 0.4 strain (b), at 0.5 strain (c)*

material constants. Q_{def} is the thermal activation energy (J/mol), and R denotes the molar gas constant. The material constants were determined to establish a constitutive equation of experimental steel using true stress-strain values obtained from the hot compression test. Equations (10), (11), and (12) resulted by taking natural logarithms of equations (7), (8), and (9) respectively.

$$\ln\sigma = \frac{1}{n1}\ln\dot{\varepsilon} + \frac{1}{n1}\left(\frac{Q_{def}}{RT} - \ln A1\right) \quad (10)$$

$$\sigma = \frac{1}{\beta}\ln\dot{\varepsilon} + \frac{1}{\beta}\left(\frac{Q_{def}}{RT} - \ln A2\right) \quad (11)$$

$$\ln\left[\sinh(\alpha\sigma)\right] = \frac{1}{n}\ln\dot{\varepsilon} + \frac{1}{n}\frac{Q_{def}}{RT} - \frac{1}{n}\ln A \quad (12)$$

The procedure for calculating material constants is shown for the strain of 0.3. The n1 and β were determined by taking average slopes of lnσ- ln $\dot{\varepsilon}$ (Fig.5a) and σ- ln $\dot{\varepsilon}$ (Fig.5b) respectively for a particular strain value. α was calculated as (α=β/n1). Calculated values of n1, β, and α were found to be 7.9, 0.0707 MPa^{-1}, and 0.0098 MPa^{-1} respectively for the strain of 0.3. Similarly, the slopes of the curves ln[sing(ασ)]- ln $\dot{\varepsilon}$ (Fig.5c) and ln[sing(ασ)]-1/T (Fig.5d) were determined to obtain Q_{def}, n, and A. The average values of Q_{def}, n, and A for strain =0.3 were found to be 408.25 $kJmol^{-1}$, 5.13, and $2.97x10^{15}$ s^{-1} respectively. The calculated values were substituted in Equation (9) to obtain Arrhenius constitutive equation to describe the high-temperature behaviour of experimental steel at 0.3 as shown in equation (13).

$$\dot{\varepsilon} = 2.97x10^{15}[\sinh(0.0098\sigma)]^{5.13}\cdot\exp\left(\frac{-408250}{RT}\right) \quad (13)$$

The effect of strain was not considered in above constitutive equation. The strain compensated Arrhenius was developed by calculating material constants at different strains from 0.1 to 0.5 using the above mentioned procedure and polynomial fitting was carried out to correlate material constants with strain. Thus, flow stress could be predicted for a given strain, strain rate, and deformation temperature in terms of temperature compensated Arrhenius equation and the Zener–Holloman (Z) by following equation (14&15).

$$Z = \dot{\varepsilon}\exp\left(\frac{Q}{RT}\right) \quad (14)$$

$$\sigma = \frac{1}{\alpha}\ln\left\{\left(\frac{Z}{A}\right)^{\frac{1}{n}} + \left[\left(\frac{Z}{A}\right)^{\frac{2}{n}} + 1\right]^{\frac{1}{2}}\right\} \quad (15)$$

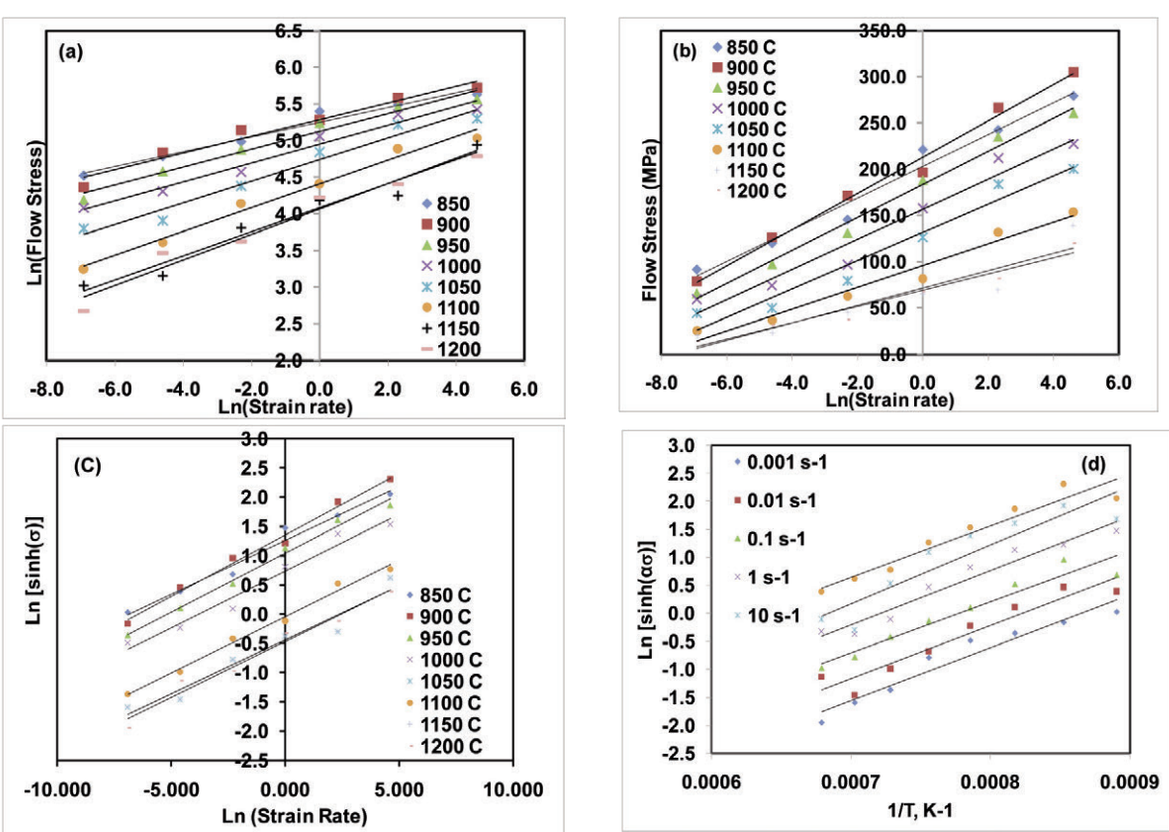

Figure 5. *Plots: (a) ln (flow stress)- ln(strain), (b) flow stress- ln(strain), (c) ln[sinh(ασ)]- ln(strain), (d) ln[sinh(ασ)]- 1/T*

Hu etal. proposed a new method to construct processing map using Arrhenius constitutive equations [9]. The proposed method used the following equations (16&17) to calculate power co-content J and η. The J was calculated by the finite integral method and its value was used to calculateh.

$$J = \oint_0^{\sigma} \varepsilon' d\sigma = \phi_0^{\sigma} A\left[\sinh(\alpha\sigma)\right]^n e^{\left(\frac{-Q}{RT}\right)} d\sigma \tag{16}$$

$$\eta = \frac{J}{J\max} = \frac{2\int_0^{\sigma} A[\sinh(\alpha\sigma)]^n e^{(-Q/RT)} d\sigma}{\sigma\dot{\varepsilon}} \tag{17}$$

The strain rate sensitivity (m) was calculated from equation (4). The differential dσ/dε̇ was calculated using equations (14 &15). The instability criteria ξ was calculated by substituting m and η in the following equation (18) proposed by Murthy etal. [7].

$$\xi = \frac{2m}{\eta} - 1 < 0 \tag{18}$$

The processing map developed using Arrhenius equation for strain value of 0.3, 0.4, and 0.5 is shown in Fig.6(a)-Fig.6(b). The processing map showed that the efficiency (η) increased consistently with increasing deformation temperature and decreasing strain rate. The efficiency varied from 14-32%. It was also observed that processing maps at different strains had a similar pattern. The instability region was demarcated by the red line and it coincided with the iso-efficiency line of 24%. Thus, it indicated that a region with efficiency < 24% indicated an instable region. The characteristics of the processing map constructed using the Arrhenius equation was different from that constructed using power law. It was inferred that the processing map based on Arrhenius constitutive equation did not give valuable information for the experimental micro-alloyed steel with respect to deformation temperature and strain rate and showed a similar efficiency pattern. The probable reason for the pattern observed was that the η and ξ were derived from the calculated flow stress at different temperatures and strain rates and lost the information from the experimental results.

3.5. Integral Equation

The Arrhenius equation representing linear variation among lns, lnε̇, and 1/T was not valid for high strain rates such as 100s$^{-1.}$ m also varied with strain rate and temperature specially for complex alloy design. The flow stress data during the hot compression test was generated from low strain rates (0.001 s^{-1}) to high strain rates (100 s^{-1}) to comprehend most of the hot working process. Murthy etal.[7, 17] described lnσ as a higher-order polynomial function of e, lnε̇, and 1/T as mentioned in equation (19). The constitutive equation was described in an empirical form and contained coefficients (C_{ijk}) to establish a good fit with the entire set of data. The measured flow

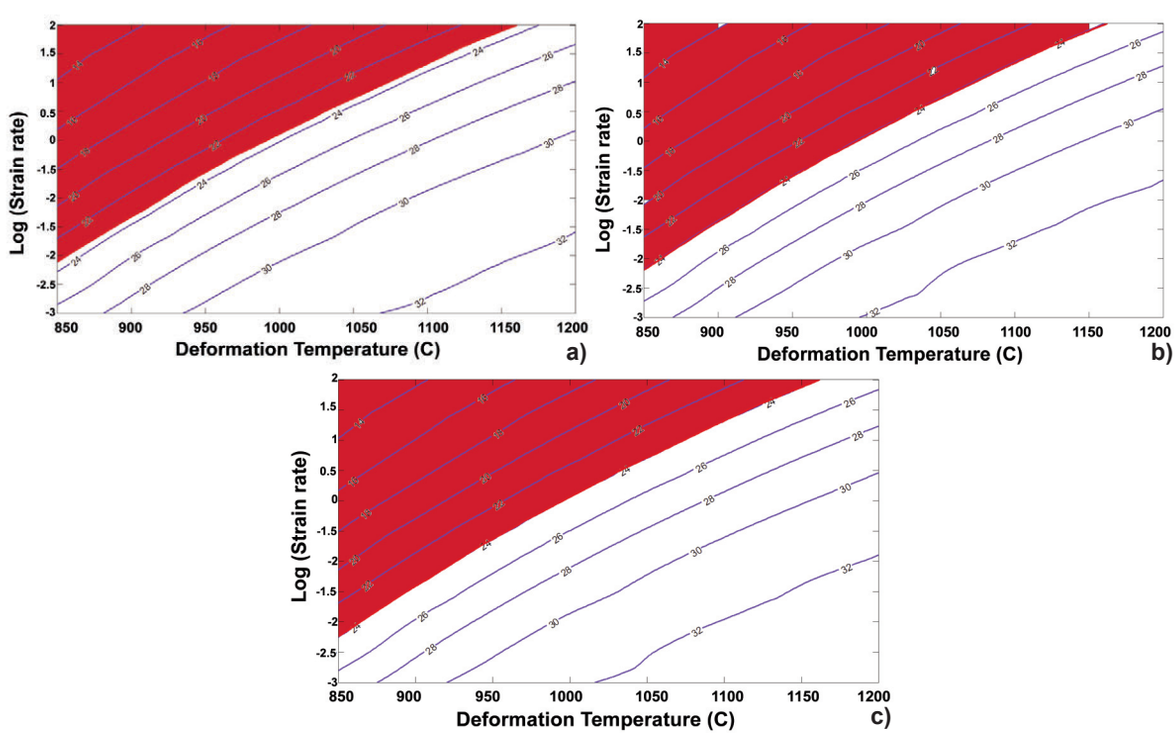

Figure 6. *Processing map using Arrhenius equation at 0.3 strain (a), at 0.4 strain (b), at 0.5 strain (c)*

stress data of experimental steel were fitted to the equation (19) to find out the constants C_{ijk} by least-squares curve fit.

$$\ln\sigma = \sum_{i=1}^{I}\sum_{j=1}^{J}\sum_{k=1}^{K} C_{ijk}\varepsilon^{i-1}\left(\frac{1000}{T}\right)^{j-1}(\ln\dot{\varepsilon})^{k-1} \quad (19)$$

The efficiency of the power dissipation map was defined by Murthy etal.[7, 17] as equation (20). Since the flow stress was generated from $\dot{e}$= 10^{-3}duringt he hot compression test, the integral in equation (20) was rewritten as given in equation (21). The first integral of equation (21) was evaluated by assuming power law for $\dot{e} \leq 10^{-3}$. The second integral in equation (21) was evaluated by generating a large number of data points using equation (19) and applying numerical integral method technique. The strain rate sensitivity (m) was calculated using equation (4) for the generated data set. The instability criteria were calculated using equation (22).

$$\eta = \frac{J}{J_{max}} = \frac{P-G}{J_{max}} = 2\left[1 - \frac{1}{\sigma\dot{\varepsilon}}\int_0^{\dot{\varepsilon}} \sigma d\dot{\varepsilon}\right] \quad (20)$$

$$\int_0^{\dot{\varepsilon}} \sigma d\dot{\varepsilon} = \int_0^{10^{-3}} \sigma d\dot{\varepsilon} + \int_{10^{-3}}^{\dot{\varepsilon}} \sigma d\dot{\varepsilon} = \left[\frac{\sigma\dot{\varepsilon}}{m+1}\right]_{\dot{\varepsilon}=10^{-3}} + \int_{10^{-3}}^{\dot{\varepsilon}} \sigma d\dot{\varepsilon} \quad (21)$$

$$\xi = \left(\frac{2m}{\eta} - 1\right) < 0 \quad (22)$$

Using Murthy etal. Method [7, 17], deformation map at strains of 0.3, 0.4, and 0.5 was constructed for the experimental micro-alloyed steel and shown in Fig.7a- Fig.7c. The iso-efficiency curves were found to be similar to curves obtained from power law. However, the peak positions were different from the power law. The iso-efficiency curves provided more accurate results compared to other methods. The instability map shown by the shaded area was also similar to the conventional power-law method, however, the instable area shown in these maps was lesser compared to the processing map constructed using power law. Hence, both power-law and the method proposed by Murthy etal. could be used to construct processing maps of micro-alloyed steel, thus establishing an accurate relationship using constitutive equations for the entire range of deformation temperature and strain rate, which is very important in representing the experimental results and constructing a meaningful processing map. A processing map constructed based on power law is a relatively simple and quick method to get the information related to the hot deformation behavior of micro-alloyed steel based on hot compression test results.

3.6. *Microstructural analysis*

The correspondence of the domains with metallurgical process obligated further endorsement by microstructural examination. The three domains of

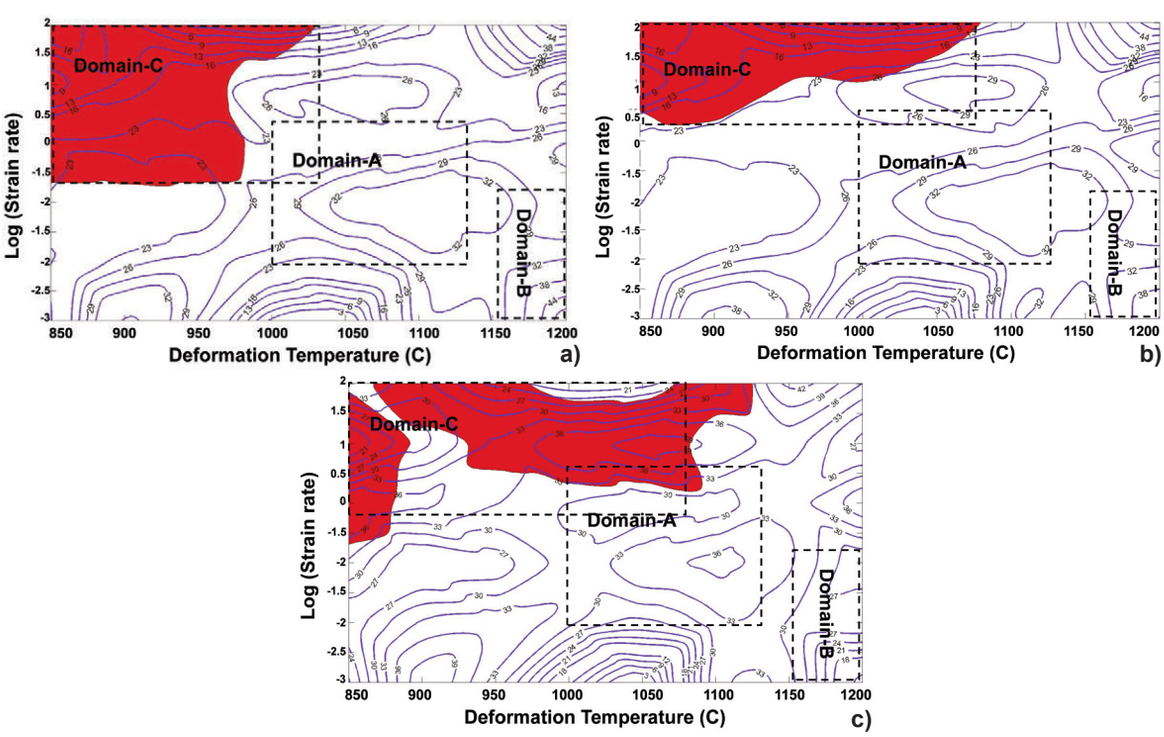

Figure 7. *Processing map by integral method at 0.3 (a), at 0.4 (b), at 0.5 (c)*

interest were already identified. These were related to dynamic recrystallization, elongated grains due to partial recrystallization, and adiabatic shear bands. These were determined as domain A, B, and C in the processing maps constructed using power law as depicted in Fig.4. Similar domains were also observed in processing maps developed using the integral method as shown in Fig.7.

The typical dynamically recrystallized microstructure from the sample deformed in Domain-A is shown in Fig.8(a). The grains were much finer and aligned along the direction normal to the deformation axis since processing was done at and above recrystallization temperature (T_{nr}: 1065°C). Processing above recrystallization temperature dominated the fine ferrite microstructures through recrystallization. The original grains got elongated during deformation and the grain boundaries became potential sites for the nucleation of new grains. The accumulation of dislocations was also the driving force for nucleation.

The microstructural changes in the temperature range of 1075-1125°Cat strain rate 1 s^{-1} corresponding to Domain-A are shown in Figs. 8 (a-c). It can be seen from Fig. 8 (a) that at the deformation temperature of 1075°C and strain rate of 1 s^{-1}, the original grains were fully recrystallized, demonstrating the occurrence of full dynamic recrystallization (DRX), and average ferrite grain size was around 5-6µm. As the deformation temperature was increased to 1100°C, the DRX grains coarsened as shown in Fig. 8 (b). As the deformation temperature was raised to 1150°C, the grain size further increased as shown in Fig. 8(c) with an average ferrite grain size in the range of 7-8µm. Fig.8(d) shows the optical micrograph of the sample deformed at 1150 ◦C at the strain rate of 0.01 s^{-1} corresponding to Domain-B conditions. In the figure elongated grains were observed, i.e. pancaked structure was generated during rolling. This was observed due to partial recrystallization. The evolved structure in Domain-B (Temp.: 1150-1200 °C & Strain rate: 0.001-0.01 s^{-1}) had high dislocation density as demonstrated in TEM analysis and dealt with later in this paper. Fig.8(e) depicts the optical micrograph of samples deformed in Domain-C conditions (900 °C & 100 s^{-1}). The adiabatic shear bands were seen in these microstructures marked by arrows. After processing in Domain-C, the structure of the evolved adiabatic shear bands comprised elongated grains, recrystallized grains, and refined grains. The evolved structure within the adiabatic shear bands was also decorated with a high density of dislocations. Hence, a high strain rate and lower deformation temperature had a considerable influence on shear strain localization and susceptibility of a material to adiabatic shear failure. Plastic deformation in Domain-C was dominated by shear strain localization along adiabatic shear bands. Cracks may initiate and propagate along these bands leading to failure during hot working [18].

3.7. Scanning Electron Microscopy (SEM)

Fig. 9(a)& 9(b) show the scanning electron micrographs of steel of Domain-A (1125◦C & 1 s^{-1}) & B (1150◦C & 0.01 s^{-1}), respectively. It may be noted that steel in Domain A showed a predominantly polygonal ferrite structure with less percentage of pearlite due to the occurrence of DRX. As far as steel in Domain-B was concerned, it is worth mentioning that ferrite grains are elongated in nature. The elongated ferrite microstructure is leading lower high angle grain boundaries as it is being confirmed in EBSD analysis [18-19].

3.8. Electron Backscatter Diffraction (EBSD) analysis

The misorientation distribution of experimental steel with deformation condition of Domain-A (1125◦C & 1 s^{-1}) and Domain-B (1150◦C & 0.01 s^{-1}) are shown in Fig. 10 (a) and 10 (b), respectively. From the misorientation distribution, deformation in Domain-A led to a structure with more high angle grain boundaries. Deformation in Domain-B led to structure with lesser high angle grain boundaries. The fraction of High-Angle Grain Boundaries (HAGBs) was around 65.15% in Domain-A while the fraction of HAGBs decreased up to 46.09% in Domain-B, because of a decrease in recrystallized ferrite and more dislocation induced during rolling. EBSD analysis showed that the percentage of high and low angle grain boundaries was dependent on deformation temperature and strain rate. High angle grain boundaries were greater in number in Domain-A compared to Domain-B due to DRX. In Doman-B the grains were not fully recrystallized and their elongated nature and high angle grain boundaries were lesser. The corresponding IPF (inverse pole figure) maps of the specimens are shown in Fig. 10(c) and 10(d), respectively. The grains were recrystallized in Domain-A, since, substantial fine and equiaxed DRX grains were found in this domain but grains were elongated in the rolling direction in Domain-B. The average grain size was15 µm in the length direction and 6 µm in the transverse direction in Domain-B [18-19].

3.9. Transmission Electron Microscopy (TEM)

TEM was carried out to explain the precipitation characteristics and dislocation density as shown in Fig.11 (a-d). The required specimens for transmission electron microscopy (TEM) were prepared by cutting thin wafers from the mid-position of the steel specimen. The thin wafer was further ground to

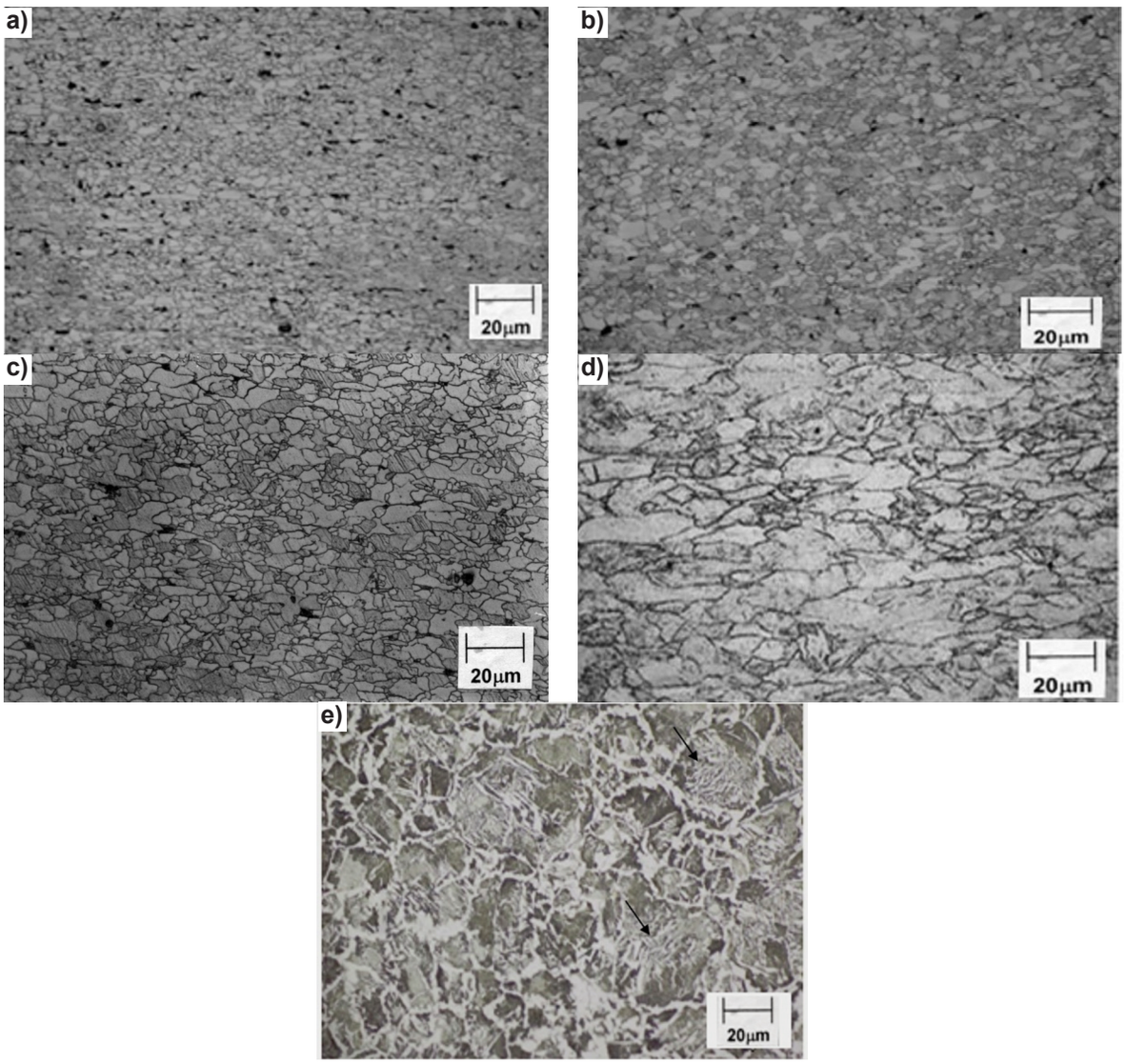

Figure 8. *Optical microstructures at different deformation Conditions (a) 1075 °C & 1 s^{-1}, (b) 1100 °C &1 s^{-1}, (c) 1125 °C & 1 s^{-1}, (d) 1150 °C & 0.01 s^{-1}, and (e) 900 °C & 100 s^{-1}*

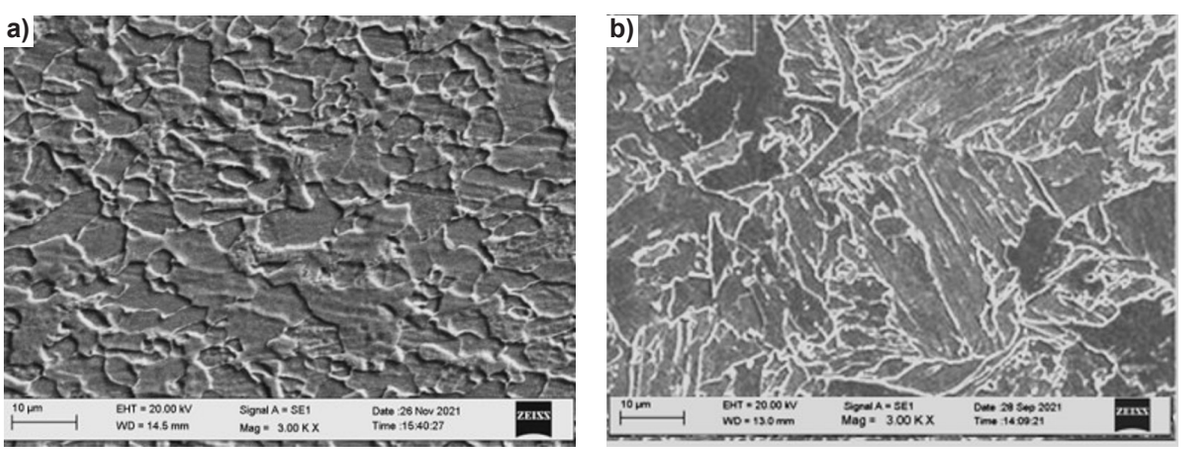

Figure 9. *(a) and (b) showing SEM micrographs of steel in Domain A& B*

around 0.1 mm in thickness. Further, discs of 3mm in diameter were grounded to a thickness of approximately 0.08 mm. The prepared specimens were further electro-polished in a jet polisher at 40 V using an electrolyte of CrO_3, acetic acid and water. TEM was conducted at 120 kV.

Fig.11(a) shows the spectrum of carbides in Domain-A (1150◦C & 1 s^{-1}) and its Energy Dispersive Spectroscopy (EDS) is depicted in Fig.(11b). Fig.11(c) shows the spectrum of carbides in Domain-B (1150◦C & 0.01 s^{-1}) and EDS is shown in Fig.(11d).A precipitate size of around 80 nm was found in Domain-

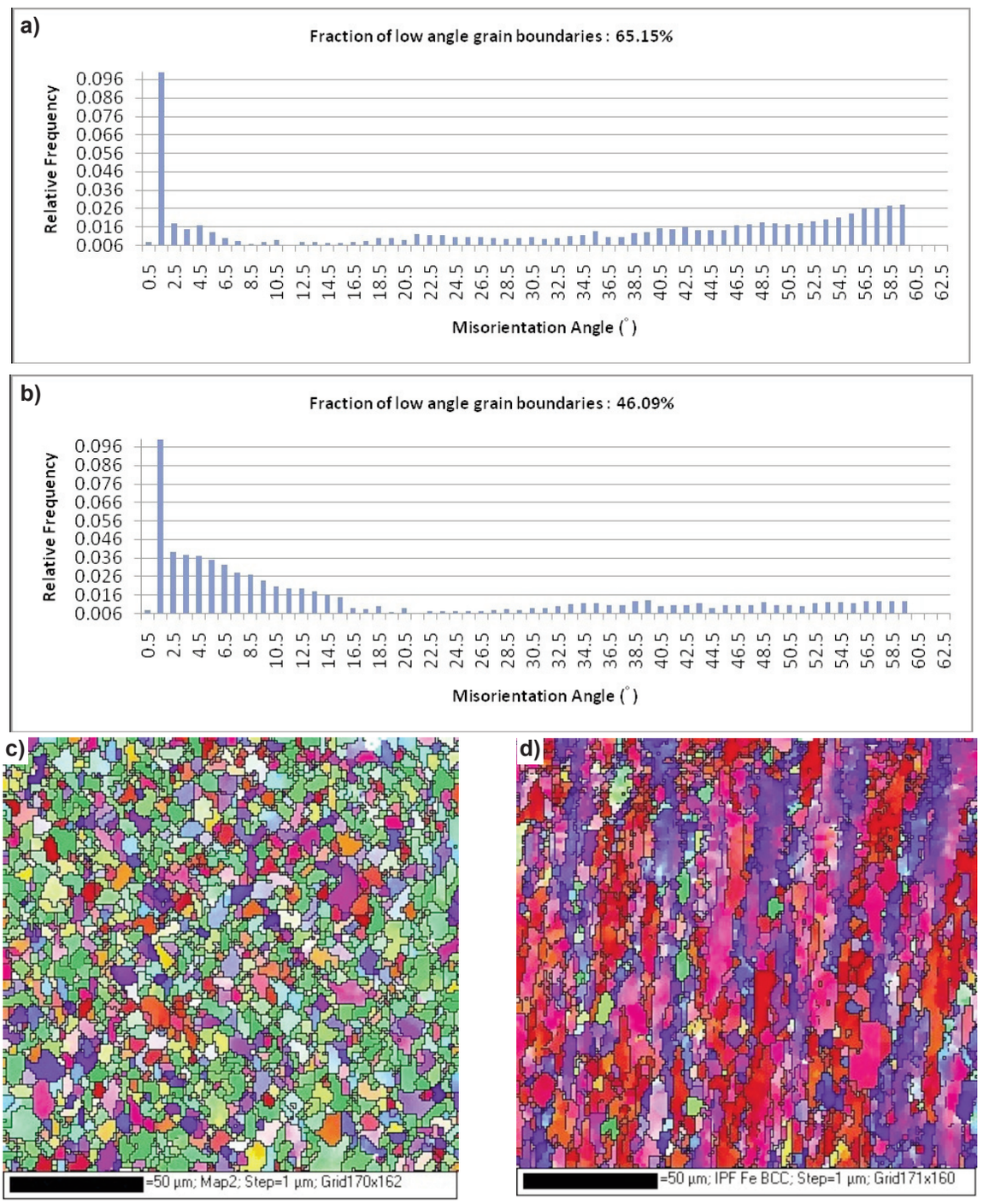

Figure 10. *(a) and (b) showing misorientation distribution related to steel in Domain A and B, (c) and (d) is showing IPF (inverse pole figure) maps related to Domain A and B*

A, it should be noted that very fine precipitates were embedded within the matrix as shown in Fig.11(a), whereas precipitate size of around 100 nm was in Domain-B with the higher surface area along with very fine precipitates of lesser numbers compared to Domain-A, as shown in Fig. 11 (c). It seems that the precipitate size in Domain-B was with a higher surface area along with lesser fine precipitates in comparison to Domain-A due to the low strain rate during deformation. The high strain rates in Domain-A led to fine precipitates along with very fine precipitates embedded within the matrix (strain-induced precipitation). Titanium and niobium were detected within the fine carbides and it was verified from its EDS spectrum as shown in Fig.11(b&d). The EDS spectra area related to both precipitates in Domain A &

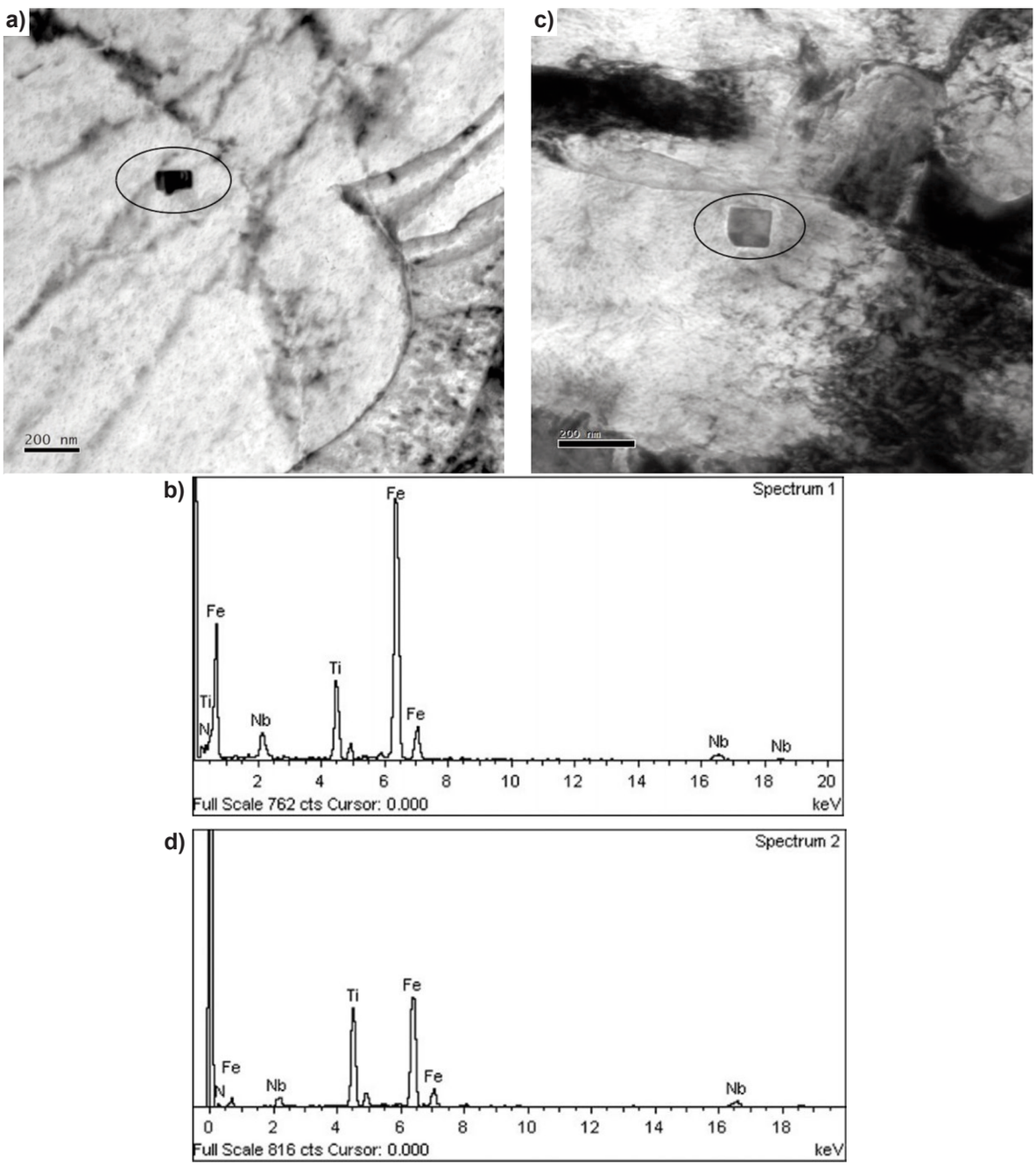

Figure 11. *Transmission electron micrographs showing carbides in experimental steel (a) bright field image showing very fine carbide deformed in Domain-A, (b) corresponding EDS spectrum of fine carbide of Domain-A(c) bright field image of fine carbide deformed in Domain-B, and (d) corresponding EDS spectrum of fine carbides of Domain-B*

B, whichever have been taken is shown with circles in Fig. 11(a&c). High dislocation density was also associated with ferrite lath in Domain-B as shown in Fig. 11 (c). As far as Domain-A was concerned, dislocations were not observed due to the occurrence of DRX. Hence, Domain-A grains were dynamically recrystallized, whereas Domain-B grains were elongated in nature and dislocation was present due to partial recrystallization [18].

4. Conclusions

Hot compression tests were carried out for micro-alloyed steel within the deformation temperature range of 850-1200°C and strain rate of 0.001- 100 s^{-1}. The experimental results were used to establish constitutive equations and construct processing maps using conventional power law, integral method, and Arrhenius equations. The following conclusions were drawn from this study:

The iso-efficiency curves in the processing map constructed based on Arrhenius constitutive equations increased continuously with an increase in deformation temperature and decrease in strain rate. Thus, information of hot workability with respect to deformation temperature and strain rate was not revealed in the processing map constructed with this method. The instability map developed by this method divided the map at efficiency ~24% and did not give relevant information with respect to the various metallurgical phenomenon.

The processing map developed based on power law and integral method provided more meaningful results and could be correlated with microstructure evolution during the deformation process. Domain-A was the safest zone where rolling was considered to be best in line with final properties requirement. This was validated by metallographic examinations through optical, SEM, TEM, and EBSD analyses.

Microstructure examination showed that DRX behaviour of this steel was dependent sensitively on the deformation temperature and strain rate, and increasing deformation temperature to1000-1150 °C and strain rate (0.01-3 s^{-1}) would lead to the more adequate proceeding of DRX.

A safe regime for hot working of the experimental microalloyed steel was found to be in the intermediate temperature-strain rate range, where the deformation process was dominated by dynamic recrystallization and dynamic recovery of the austenitic phase. This domain fell in the temperature range 1000-1150°C and strain rate range 0.01-3 s^{-1}

Acknowledgment

The authors are grateful to the management of R&D Centre for Iron & Steel, Steel Authority of India Ltd., Ranchi for their encouragement and support during the execution of the present work.

Author's Contributions

The authors confirm contributions to the paper as follows: study conception and design: Alok Kumar Das, Bimal Kumar Jha, Experimentation and compilation of data: Suman Kant Thakur, Mathematical modelling and development of deformation map: Suman Kant Thakur, Bimal Kumar Jha, Analysis and interpretation of results: Suman Kant Thakur, Bimal Kumar Jha, Alok Kumar Das; Draft manuscript preparation: Suman Kant Thakur. All authors reviewed the results and approved the final version of the manuscript.

Data Availability

The processed data required to reproduce these findings are available to download from [Thakur, Suman (2021), "Flow Stress Data", Mendeley Data, V1, doi: 10.17632/ghn2rd47xx.1, http://dx.doi.org/10.17632/ghn2rd47xx.1].

Conflict of Interest

The authors declare that they have no known competing financial interests or personal relationships that could have appeared to influence the work reported in this paper

References:

[1] K.P. Rao,Y.V.R.K. Prasad, K. Suresh, Hot working behavior and processing map of a γ-TiAl alloy synthesized by powder metallurgy, Materials & Design, 32(10) (2011) 4874-4881. https://doi.org/10.1016/j.matdes.2011.06.003

[2] M.S. Popkiadeh, A. Rezaeian, G. Dini, M. R. Toroghinejad, Hot deformation behavior of high Mn TWIP steel using Processing Map, ISIJ International, 55 (3) (2015) 691-696. https://doi.org/10.2355/isijinternational.55.691

[3] H.Q. Huang, H.S. Di, N. Yan, J.C. Zhang, Y.G. Deng, R.D.K. Misra, J.P. Li. Hot deformation behavior and processing maps of a high Al-low Si transformation-induced plasticity steel: Microstructural evolution and flow stress behavior, Acta Metallurgica Sinica(English Letters), 31(5) (2018) 503-514. https://doi.org/10.1007/ s40195-017-0676-2

[4] N. Li, W. Kingkam, R. Han, Y. Huang, Y. Li, Y. Zhu, Z. Bao, H. Zhang, C. Zhao, Processing maps for hot working of HSLA pipeline steel, Materials Research Express, 6 (2020). https://doi.org/10.1088/2053-1591/ab6768.

[5] Y.V.R.K. Prasad, Processing maps: A status report, Journal of Materials Engineering and Performance, 12 (2003) 638–645. https://doi.org/10.1361/105994903322692420.

[6] Y. Prasad, T. Seshacharyulu, Modeling of hot

deformation for microstructural control, International Materials Reviews, 43(6) (1998) 243-258. https://doi.org/ 10.1179/imr.1998.43.6.243

[7] S.V.S.N. Murty, B.N. Rao, B.P. Kashyap, Development and validation of a processing map for zirconium alloys, Modelling and Simulation in Material Science and Engineering, 10 (2002) 503–520. https://doi.org/10.503.10.1088/0965-0393/10/5/303.

[8] G. Quan, Y. Shi, C. Yu, J. Zhou, The improved Arrhenius model with variable parameters of flow behaviour characterizing for the as-cast AZ80 magnesium alloy, Journal Materials Research, 16(4) (2013) 785-971. https://doi.org/10.1590/S1516-14392013005000070

[9] M. Hu, L. Dong, Z. Zhang, X. Lei, R. Yang, Y.Sha, A novel computational method of processing map for Ti-6Al-4V alloy and corresponding microstructure study, Materials, 11(2018) 1599. https://doi.org/10.3390/ma11091599

[10] H. Zhao, J. Qi, R. Su, H. Zhang, H. Chen, L.Bai, C. Wang, Hot deformation behaviour of 40CrNi steel and evaluation of different processing map construction methods, Journal of Materials Research & Technology, 9(3) (2020) 2856-2869. https://doi.org/ 10.1016/j.jmrt.2020.01.020

[11] S.G. Hong, K.B. Kang, C.G. Park, Strain-induced precipitation of NbC in Nb and Nb-Ti microalloyed HSLA steels, Scripta Materialia, 46 (2) (2002) 163–168. https://doi.org/ 10.1016/ S1359-6462(01)01214-3

[12] J. Luo, M.Q. Li, Y.G. Liu, H.M. Sun, The deformation behavior in isothermal compression of 300M ultrahigh-strength steel, Materials Science & Engineering A 534 (2012) 314–322. https://doi.org/10.1016/ j.msea.2011.11.075

[13] R.L. Goetz, S.L. Semiatin, The adiabatic correction factor for deformation heating during the uniaxial compression test, Journal of Materials Engineering and Performance, 10(6) (2001) 710-717. https://doi.org/10.1361/105994901770344593

[14] J. Zhao, Z. Jiang, Thermo-mechanical processing of advanced high strength steels, Progress in Materials Science, 94 (2018) 174-242. https://doi.org/10.1016/J.PMATSCI.2018.01.006

[15] W. Wang, J. Zhao, R. Zhai, R. Ma, Arrhenius-type constitutive model and dynamic recrystallization behavior of 20Cr2Ni4A alloy carburizing steel, Steel Research International, 88 (3) (2016). https://doi.org/10.1002/srin.201600196

[16] S.K. Thakur, L. Harish, A.K. Das, S. Rath, P. Pathak, B. K. Jha, Hot deformation behavior and processing mp of Nb-V-Ti micro-alloyed steel, Materials Today: Proceedings 28 (2020) 1973–1979. https://doi.org/10.1016/ j.matpr.2020.05.566

[17] S.V.S.N. Murthy, B.N. Rao, B.P. Kashyap, Development and validation of a processing map for AFNOR 7020 aluminium alloy, Materials Science and Technology,20 (2004) 772-782. https://doi.org/10.1179/026708304225016671

[18] P. Qian, Z. Tang, L. Wang, C. W. Siyasiya, Hot deformation characteristics and 3-D processing map of a high-titanium Nb-micro-alloyed steel, Materials 2020, 13, 1501. https://doi.org/10.3390/ma13071501

PONAŠANJE MIKROLEGIRANOG ČELIKA TOKOM PLASTIČNE DEFORMACIJE NA ODREĐENOJ TEMPERATURI NA MAPI PROCESA DOBIJENOJ NA OSNOVU RAZLIČITIH KONSTITUTIVNIH JEDNAČINA

S. K. Thakur [a,b,*], A. K. Das [b], B. K. Jha [c]

[a] Steel Authority of India Ltd., Centar za istraživanje i razvoj, Ranči, Indija
[b] IIT(ISM), Mašinsko inženjerstvo, Danbad, Indija
[c] Državni institut za tehnologiju livenja i kovanja, Odeljenje za materijale i metalurgiju, Ranči, Indija

Apstrakt

Obradivost mikrolegiranog čelika je ispitivana u temperaturnom opsegu deformacije od 850 – 1200 °C i brzini deformacije od 0,001 - 100 s^{-1}. Uspostavljen je odnos između promene napona i temperature, brzine deformacije i same deformacije da bi se konstruisale mape procesa obrade mikrolegiranog čelika. Mape su konstruisane pomoću konvencionalnog zakona snage, metode integrala i Arenijusove jednačine. Dobijene mape procesa su korišćene za predviđanje optimalnih uslova za toplotnu deformaciju i potvrđene su metalurškim ispitivanjima. Utvrđeno je da se siguran režim za obradu eksperimentalnog čelika nalazi u srednjem opsegu odnosa temperatura-deformacija (1000-1150 °C; 0,001-10 s^{-1}) tokom kojeg je bila dominantna dinamička rekristalizacija i oporavak austenitne faze. Mapa procesa dobijena na osnovu Arenijusove jednačine nije otkrila relevantne informacije o obradivosti čelika u odnosu na temperaturu i brzinu deformacije. Na ponašanje tokom dinamičke rekristalizacije na eksperimentalni čelik je uticaj imala i temperatura i brzina deformacije, što je detaljnije objašnjeno ispitivanjem mikrostrukture.

Ključne reči: *Deformacija; Mapa procesa; Mikrolegure; Arenijusova jednačina*